Acta Oceanol. Sin., 2023, Vol. 42, No. 11, P. 146–158
https://doi.org/10.1007/s13131-022-2113-2
http://www.aosocean.com
E-mail: ocean2@hyxb.org.cn

Study on strength properties and soil behaviour type classification of Huanghe River Delta silts based on variable rate piezocone penetration test

Yunuo Liu[1, 2], Guoqing Lin[1, 2], Yan Zhang[3, 4*], Shenggui Deng[3, 4*], Lei Guo[5], Tao Liu[1, 2, 6]

[1] Shandong Provincial Key Laboratory of Marine Environment and Geological Engineering, Ocean University of China, Qingdao 266100, China

[2] College of Environmental Science and Engineering, Ocean University of China, Qingdao 266100, China

[3] Key Lab of Submarine Geosciences and Prospecting Techniques MOE China, Ocean University of China, Qingdao 266100, China

[4] College of Marine Geosciences, Ocean University of China, Qingdao 266100, China

[5] Institute of Marine Science and Technology, Shandong University, Qingdao 266237, China

[6] Qingdao National Laboratory for Marine Science and Technology, Qingdao 266100, China

Received 3 March 2022; accepted 15 August 2022

Abstract

Fine-grained silt is widely distributed in the Huanghe River Delta (HRD) in China, and the sedimentary structure is complex, meaning that the clay content in the silt is variable. The piezocone penetration test (CPTu) is the most widely approved *in situ* test method. It can be used to invert soil properties and interpret soil behavior. To analyse the strength properties of surface sediments in the HRD, this paper evaluated the friction angle and its inversion formula through the CPTu penetration test and monotonic simple shear test and other soil unit experiments. The evaluation showed that the empirical formula proposed by Kulhawy and Mayne had better prediction and inversion effect. The HRD silts with clay contents of 9.2%, 21.4% and 30.3% were selected as samples for the CPTu variable rate penetration test. The results show as follows. (1) The effects of the clay content on the tip resistance and the pore pressure of silt under different penetration rates were summarized. The tip resistance Q_t is strongly dependent on the clay content of the silt, the B_q value of the silt tends to 0 and is not significantly affected by the change of the CPTu penetration rate. (2) Five soil behavior type classification charts and three soil behavior type indexes based on CPTu data were evaluated. The results show that the soil behavior type classification chart based on soil behavior type index I_{SBT}, the Robertson 2010 behavior type classification chart are more suitable for the silty soil in the HRD.

Key words: Huanghe River Delta, piezocone penetration test, silty soils, clay content, friction angle, soil behaviour type classification

Citation: Liu Yunuo, Lin Guoqing, Zhang Yan, Deng Shenggui, Guo Lei, Liu Tao. 2023. Study on strength properties and soil behaviour type classification of Huanghe River Delta silts based on variable rate piezocone penetration test. Acta Oceanologica Sinica, 42(11): 146–158, doi: 10.1007/s13131-022-2113-2

1 Introduction

Silty seabeds are found throughout the world's undersea construction areas, such as Gingin and Burswood in Australia, Opelika in North America, the Huanghe River Delta (HRD) and Hangzhou Bay (Brandon et al., 2006; Geiser et al., 2006). The HRD is located to the south of the Bohai Sea. More than 90% of its surface sediments are silty soil (Feng et al., 2002). It is successful economic zone and an ecological and environmental protection zone of the "Yellow and Blue Strategy", and also the main oil production area of Shengli Oilfield, which is an area of potential geological activities that could cause geological disasters during offshore construction (Qi and Liu, 2017; Wang and Liu, 2016). The seabed of the HRD is dotted with pipelines and cables for the production of oil and natural gas (Song et al., 2020). In recent years, engineering accidents with varying degrees of severity have occurred in the region, and instability of the seabed has resulted in significant economic and social costs. Sediment characteristics are closely related to the physical and mechanical properties of the sediments and geological hazards (Yang et al., 2019). Therefore, it is necessary to explore the *in-situ* mechanical properties and characteristics of the surface sediments in the region, which is of great significance to the evaluation of geological disasters and structural safety.

The piezocone penetration test (CPTu) has been proven to be more reliable, cost effective and valuable in characterizing subsurface conditions and in assessing various soil properties (Shahri et al., 2015). Previous studies have used the cone penetration test (CPT) data to establish correlation formulas and derive soil properties, and CPT is also suitable for soil behaviour type classification and formation profile analysis, where extensive parameter inversion can be performed directly from the measured data (Robertson, 2009; Schneider et al., 2008). As an

Foundation item: The National Natural Science Foundation of China under contract No. U2006213.
*Corresponding author, E-mail: zhangyan4850@ouc.edu.cn; dengsg@ouc.edu.cn

important parameter in soil mechanical analysis, friction angle is used to calculate erosion, bearing capacity, and shear strength of seabed sediments in offshore analysis (Albatal et al., 2020). It is therefore reasonable and necessary to use CPTu to study the soil behaviour type classification method and inversion of friction angle in the HRD.

The hydrodynamic conditions of the HRD are complex, and the viscous sediment is widely distributed (Wen et al., 2018). The clay content in the nearshore is low, where the sediment rapidly accumulates, while the clay content is higher far from the shore (Cheng and Xue, 1997). The clay content in silty soil varies and affects the soil to some extent. For example, different clay mass fractions in saturated silty soil have different effects on the adsorption or flow of water, thus affecting the change in the pore water pressure of the soil (Liu et al., 2012). Previous studies on the effect of clayey content on the CPTu penetration test have been inadequate, however. Moreover, several researchers studying the rate effects in silt have highlighted the sensitivity of the penetration rate to the engineering strength parameters (Tonni and Gottardi, 2011; Holmsgaard et al., 2016; Zhang et al., 2022c). Furthermore, the penetration rate in different soils has different effects on the test results. To explore the different soils distributed in the HRD, therefore, the CPTu variable rate penetration test was conducted for silty soils with different clay contents. To explore the different soils distributed in the HRD and the penetration rate most suitable for detecting the clay content of silt in the HRD, therefore, the CPTu variable rate penetration test was conducted for silty soils with different clay contents.

Soil behavior type classification is based on the common qualities or characteristics of soils. To obtain the clay content in the HRD area, which can be used to determine the properties of the soil, and the use of CPT for soil classification is more rapid and effective than other methods. There are several soil behavior type classification methods to predict soil type and state using CPT or CPTu data (Begemann, 1965; Douglas and Olsen, 1981; Jones and Rust, 1982; Senneset and Janbu, 1985; Robertson et al., 1986; Robertson, 1990, 2009; Eslami and Fellenius, 1997; Brouwer, 2007), the proposed charts by Robertson et al. (1986) and Robertson (1990) have been popular and widely used (Long, 2008; Cai et al., 2011). Based on the common soil behavior type classification methods mentioned above, this paper analyses the data collected by the CPTu for silt with different clay contents in the HRD under the standard penetration rate finds out the soil behavior type classification methods suitable for the HRD and the influence of penetration rate, which provides useful guidance for geotechnical engineers.

2 Strength properties of remodeling HRD silts

The silt samples used in the test were taken from shallow tidal flats in Dongying City, Shandong Province, and a particle analysis test was carried out on the samples. The particle distribution curve is shown in Fig. 1. The silt from the HRD contains clay content of 9.2%.

The physical properties of the HRD silts are shown in Table 1, which can be used as reference for subsequent soil sample preparation.

The soil samples of the one-dimensional compression test were obtained by the slurry deposition method. Figure 2 shows the vertical consolidation coefficient (c_v) versus σ_v. The soil

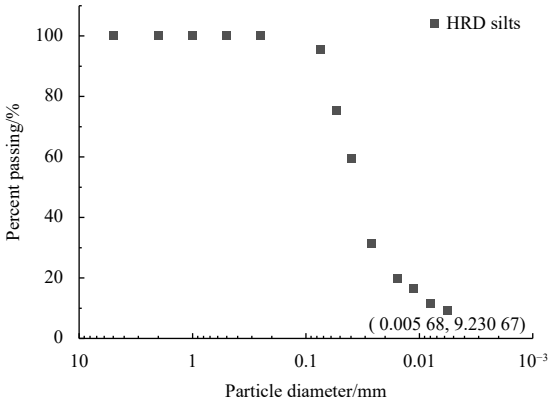

Fig. 1. Grain distribution curves of Huanghe River Delta (HRD) silts.

samples of the CPTu pressure chamber tests were also obtained by the slurry deposition method. Thus, it was convenient to obtain c_v of the soil under a known upper stress in the subsequent analysis, which is of help to the inversion analysis in the pressure chamber tests. Consolidation coefficients of HRD silts are summarized in Table 2.

The Sheartra-II instrument used in monotonic simple shear test is shown in Fig. 3 below. The samples with diameter of 70 mm and height of 20 mm were prepared. A cylindrical soil specimen is laterally confined by low friction retaining rings, ensuring a constant cross sectional area. The shear rate is set as 0.02 mm/min according to the ASTM D6528-17 Standard Test Method for Consolidated Undrained Direct Simple Shear Testing of Fine Grain Estuary (2017). The initial vertical stresses were set as 30 kPa, 90 kPa and 100 kPa, respectively.

Figure 4 shows the results of monotonic simple shear test for the HRD silts consolidated under different initial vertical stress, in which the effective stress paths, the stress-strain curves and the excess pore pressure-strain responses are presented. σ'_{v0} is vertical stress, τ is shear stress, γ is shear strain and u_w is excess pore pressure.

Under the condition of low stress, the dilatancy of soil is enhanced (Zhang et al., 2022a). When the initial vertical stress is less than 100 kPa, the HRD silts follow a similar effective stress path. (1) The sample volume is decreased at early stage of shearing and then increases with increasing shear strain. To keep the height of the sample unchanged, the vertical stress decreases initially corresponding to the increased pore pressure. With the decrease of initial vertical stress, the shear strain at the peak excess pore pressure is decreased. The corresponding strains are 2%, 3% and 3% for samples under 30 kPa, 90 kPa and 100 kPa, respectively. (2) Then the stress path reaches the phase transition point, as shown in Fig. 4a. The sample volume then expands, the vertical stress increases to keep the volume unchanged. The sample shows strain hardening without an apparent failure point, and the stress path eventually moves along a straight line. (3) Under the three initial vertical stress, the initial contractive tendency and then dilatant tendency are captured by the increased and decreased excess pore pressure, respectively. The lower excess pore pressure means that dilatant tendency of samples is more remarkable and the effective stress is higher. Therefore, samples

Table 1. Soil properties of Huanghe River Delta silts

Soil type	Specific gravity	Water content/%	e_{max}	e_{min}	ρ'/(g·cm^{-3})	Liquid limit/%	Plastic limit/%	Plasticity index I_p/%
ML	2.70	25.4	1.45	0.45	1.25	29.6	21.6	9.8

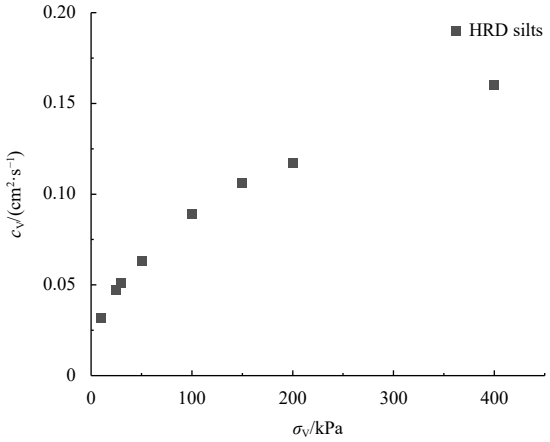

Fig. 2. One-dimensional compression test results.

Table 2. Consolidation coefficient (C_v) of Huanghe River Delta silts

Vertical stress	30 kPa	50 kPa	100 kPa	150 kPa
c_v/(cm²·s⁻¹)	0.051	0.063	0.089	0.106

Fig. 3. The ShearTrac-II System.

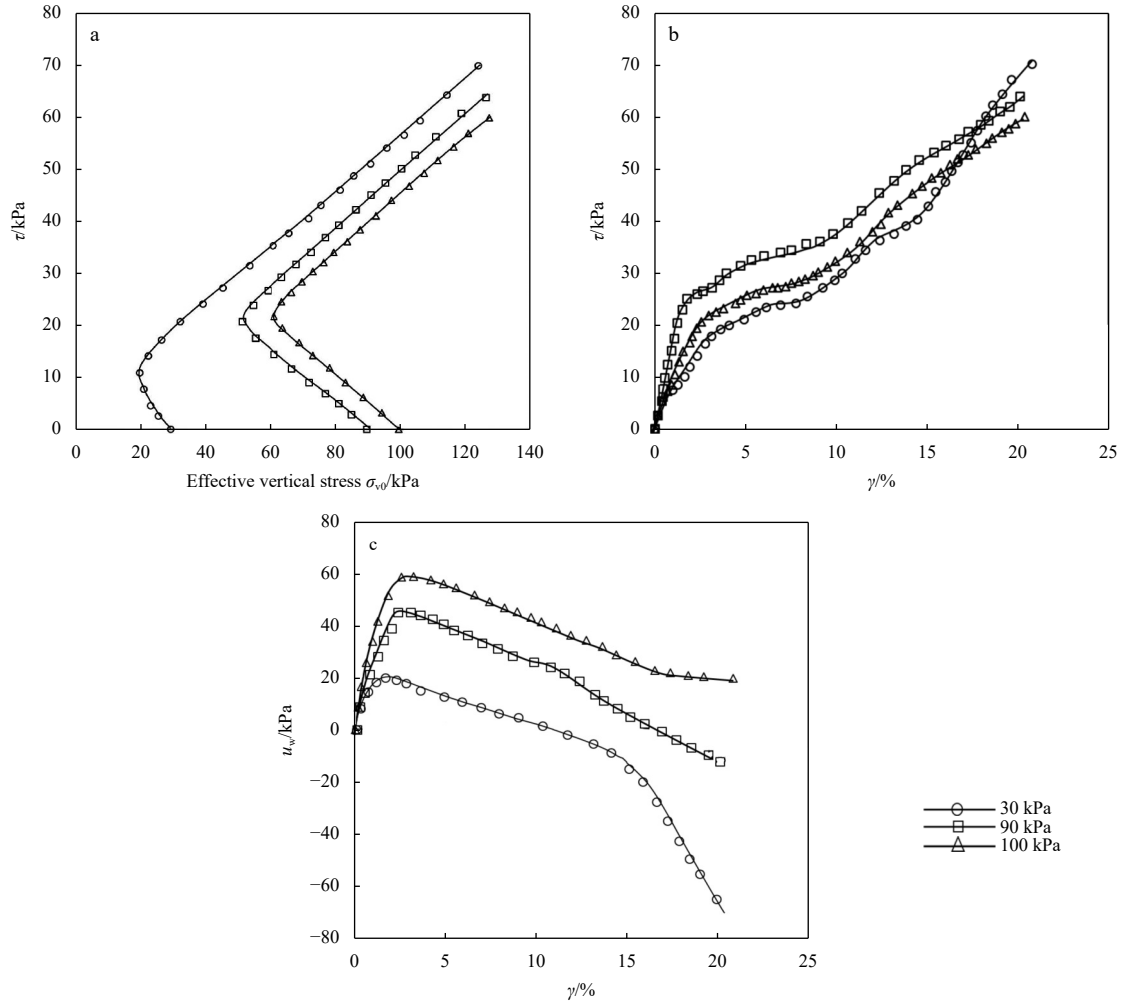

Fig. 4. Monotonic shearing test results: the effective stress path (a), stress-strain relationship (b), equivalent excess pore pressure-strain relationship (c).

with the initial vertical stress of 30 kPa show a higher shear strength eventually even exceeds the shear stress under initial vertical stress of 90 kPa and 100 kPa.

3 Pressure chamber tests

3.1 *Test equipment*

3.1.1 *Laboratory penetration test system*

Figure 5 shows a photograph of the penetration test equipment in the laboratory, including the calibration chamber and the velocity control penetration system. The penetration rig is controlled by a servo motor. The penetration rate of CPTu and penetration depth in the calibration chamber are controlled by setting the data in the control system.

3.1.2 *Micro CPTu*

The micro CPTu device used in this experiment is shown in Fig. 5. The device can accurately measure the numerical changes of tip resistance (q_c), sleeve friction resistance (f_s) and pore water pressure (u_2). In the calibration chamber test, the CPTu diameter (d) was 16 mm, the cone angle was 60°, the friction bucket area was 30 cm^2, and the area ratio was 0.53. The miniature cone used in this study is a subtracted CPTu, in which both the cone and the sleeve produce compression force on the weighing sensors in series. As shown in Fig. 6, the tip resistance, sleeve friction resistance and pore water pressure are measured directly by force sensors and pore pressure sensors. The cable through the hollow steel shaft is connected to the cone head and to the conical penetrometer actuator. The maximum range of resistive pressure measuring element on the cone top is 12 MPa, the maximum range of the sleeve friction resistance is 0.75 MPa, and the maximum range of the pore pressure sensor is 350 kPa.

3.2 *Equipment stability and accuracy*

To ensure the accuracy of the test, a penetration test was conducted of Malaysian kaolin before the formal test, and then the test results were verified with the previous test results to determine whether the accuracy of the test device met the requirements.

The methods to calculate the corrected pore pressure parameter ratio B_q and penetration rate V are as follows:

$$V = \frac{vd}{c_v}, \tag{1}$$

$$B_q = \frac{u_2 - u_0}{q_t - \sigma'_{v0}}, \tag{2}$$

where, v is penetration rate; d is probe diameter; and c_v is coefficient of consolidation; u_2 is the penetration pore pressure; u_0 is the current *in situ* water pressure; and $q_t - \sigma'_{v0}$ is the net cone tip resistance, q_t is correct cone resistance, σ'_{v0} is the current in situ total vertical stres.

The test results were essentially consistent, as shown in Fig. 7, indicating that the CPTu penetration system used in this study has sufficient test accuracy to meet the test requirements and produce reliable test results. The experiment was therefore designed as described in the following sections.

3.3 *Test procedures*

3.3.1 *Soil preparation and consolidation*

According to previous studies, the main component of low plastic silt is non-plastic silt (0.005–0.075 mm). The clay content of silty soil in the HRD is generally 5%–30%, and the sediment has obvious zonation. The general trend is that the clay content is lower near the shore, while the clay content increases further from the shore.

The test soil samples were prepared by the slurry consolidation method. The clay minerals in the silt of HRD are mainly illite, kaolinite and montmorillonite (Wang et al., 2008). Based on that, we added a certain proportion of kaolin, illite and montmorillonite to the remolded HRD silt with clay content of 21.4% and 30.3%. According to the main types of clay of the HRD silts, a certain proportion of kaolin, illite and montmorillonite were added to the remolded clayey silt with clay content of 21.4% and 30.3%. The particle distribution curve is shown in Fig. 8. The dry particles of the silt and types of clay minerals calculated and configured were initially mixed with deionized water, then transferred into the mud-mixing preparation system. After fully mixed

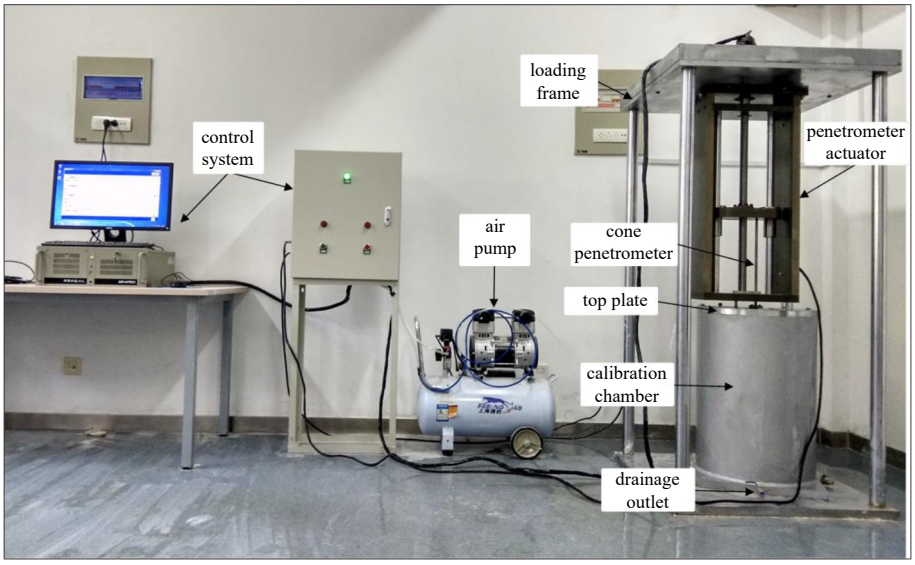

Fig. 5. The laboratory penetration test system.

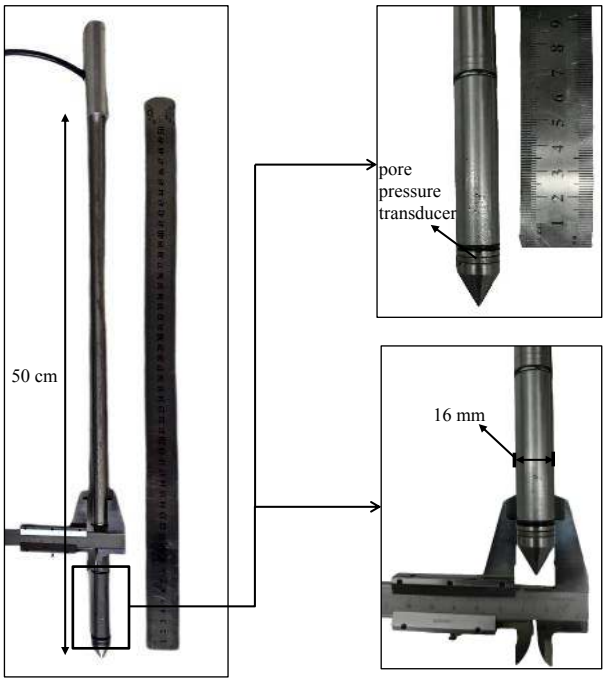

Fig. 6. Micro-CPTu.

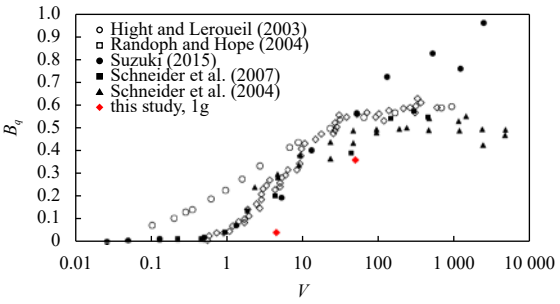

Fig. 7. Comparisons of penetration test results in Malaysian kaolin.

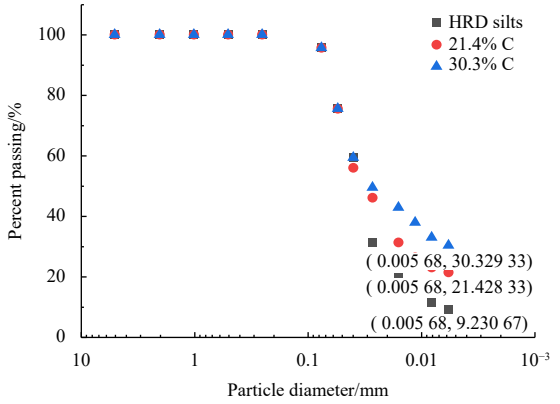

Fig. 8. Grain distribution curves of Huanghe River Delta (HRD) silts with different clay content.

and vacuum saturated, the saturated mud was collected. The mixing process was carried out in a vacuum for about 4 h.

Before the saturated slurry was transferred into the consolidation drum, the sand layer and filter paper were laid at the bottom, and silicon grease was evenly daubed on the wall of the consolidation drum, to reduce the friction between the saturated slurry and the consolidation drum. The slurry was poured into the consolidation apparatus with care to avoid bubble retention. The drainage pipe was closed throughout the process. After the drum was filled to the maximum level, the filter paper and geotextile were spread on the top of the slurry to provide the upper drainage layer. Then the load-board was fixed, and the hydraulic cylinder with reaction frame was installed. Next, the drainage pipe was opened, and the slurry was consolidated under progressively increased pressure. The displacement sensor was used to collect data once a day until the next level of loading was carried out after the settlement displacement of the soil sample was stable. In the consolidation process, the water level was maintained above the load-board to ensure that the soil sample reached full saturation after consolidation.

The soil samples with different clay contents were taken out by a sampler for the consolidation test. The consolidation effect and consolidation coefficient were measured. Figure 9 shows the c_v versus σ_v of silt with different clay contents. With the increase of σ_v, the multiple of the difference increases. When σ_v is in the range 30–200 kPa, the c_v of silty soil is 0.051–0.158 cm^2/s, that of 20% clay content is 0.027–0.053 cm^2/s, and that of 30% clay content is 0.002–0.005 cm^2/s. The consolidation coefficient decreases with the increase of clay particles under the same stress state. The soils exhibited increased compressibility and reduced consolidation characteristics with increasing clay content.

3.3.2 *Penetration procedures*

The penetration procedure involved the following steps.

(1) Before the penetration, calibrate the force sensor with a calibration device and saturate the porous filter of the pore pressure sensor.

(2) Move the penetration device above the consolidation device, connect the micro-CPTu and the penetration device, adjust the position so that the micro-CPTu is located at a certain distance above the reserved penetration hole in the load-board, and then set the penetration depth and speed according to the distance from the reserved hole position.

(3) Remove the filter paper in the hole before infiltration to prevent the paper being brought into the soil; open the data measurement and acquisition program; start the penetration device, and run the pre-set penetration program to complete the penetration, until the target depth stop.

(4) Press the reset button; remove the mini-CPTu from the soil; remove the soil on the micro-CPTu probe rod; move the

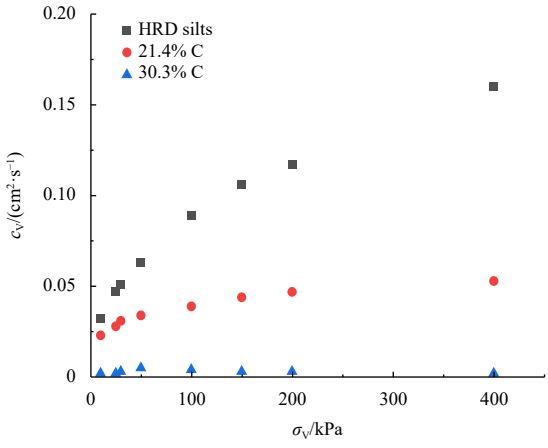

Fig. 9. One-dimensional compression test results of Huanghe River Delta (HRD) silts with different clay content.

device to the next reserved hole; and repeat the steps above. The penetration interval of each reserved hole is 24 h.

3.4 *Test plans*

In view of the impact of different penetration rates and clay contents on the test results, three groups of penetration experiments with different rates (0.2 mm/s, 1 mm/s, 10 mm/s and 20 mm/s) were carried out for three groups of silt with clay contents of 9.2%, 21.4% and 30.3%. CPTu penetration data in the early stage was unstable, so the stable stage was selected as the "zone of interest" (Suzuki, 2015) and the data of this stage were used for analysis.

4 Results and discussion

4.1 *Friction angle*

In the monotonic simple shear test, peak friction angle can be obtained from the effective stress path. It can be expressed as

$$\varphi' = \arcsin\left(\frac{\tau}{\sigma_{\mathrm{v}}}\right). \tag{3}$$

The slope M of the critical state line of soil can be obtained by the following formula:

$$\mathrm{M} = \frac{6\ \sin\varphi'}{3-\sin\varphi'}. \tag{4}$$

Table 3 shows the peak friction angles under different initial vertical stresses. Since the load of CPTu penetration test is 30 kPa, the value obtained under initial vertical stress of 30 kPa is selected for comparison with CPTu inversion data.

Although the friction angle can be obtained by laboratory test, it is not as direct, fast and convenient as the *in-situ* test method. Therefore, it is necessary to find the inversion formula of friction angle suitable for the HRD. The relationship between q_t and penetration depth (h) under different CPTu penetration rates of soils with different clay contents is shown in Fig. 10.

Table 3. Friction angle obtained from monotonic shear test

$\sigma'_{\mathrm{v_0}}$/kPa	φ'/(°)	M
30	32.34	1.30
90	30.17	1.21
100	27.96	1.11

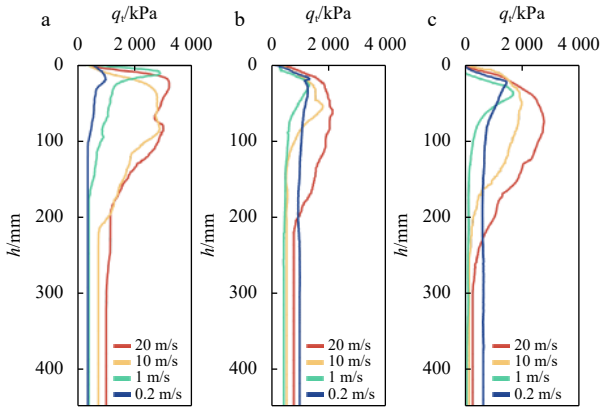

Fig. 10. Test results q_t vs. h: remolded Huanghe River Delta silts (a); 20% C mixture (b); 30% C mixture (c).

q_t is calculated by the following formula:

$$q_t = q_c + u_2\left(1 - A_a/A_c\right), \tag{5}$$

where q_c is the measured tip resistance value. A_a and A_c are the cross-sectional areas of the top column and the bottom of the cone respectively. In this paper, the A_a/A_c of the CPTu used in the test is 0.53.

According to previous studies, the internal friction angle obtained by CPT data inversion is usually the peak friction angle, φ'. Several methods have been established to estimate the peak friction angle (φ') of soil using either empirical or semi-emperical methods, bearing capacity theory, or cavity expansion theory. For example, using the bearing capacity theory, Mitchell and Lunne (1978) studied the relationship between q_c and $\varphi'$of the CPT. Lunne and Christophersen (1983), and Robertson and Campanella (1983) compared the q_c obtained from the pressure chamber test with the drainage triaxial test results φ' of the same sand, and produced a relationship diagram of the bearing capacity coefficient.

Kulhawy and Mayne (1990) proposed an alternative expression of peak friction angle to explain the nonlinear normalization of cone resistance with stress level. The test results are compared with the triaxial test results (Finke et al., 2001). It is proved that the method has good effect in silty soil.

$$\varphi' = 17.6^\circ + 11.1\lg\left(\left(\frac{q_c}{p_{\mathrm{a}}}\right)\cdot\left(\frac{p_{\mathrm{a}}}{\sigma'_{\mathrm{v0}}}\right)^{0.5}\right). \tag{6}$$

In the Eq. (6), p_{a} is the atmospheric reference pressure.

Mayne (2006) proposed a formula to calculate φ'. It has been adopted by many geotechnical engineers and can be expressed as follows:

$$\varphi' = \arctan(0.1 + 0.381\lg(q_c/\sigma'_{\mathrm{v0}})). \tag{7}$$

This paper uses the two formulas above as inversion formulas. When the probe penetrates to a certain depth, it is no longer affected by the interference of the boundary soil, and so the parameters used in the inversion formula were selected from the stable section. Furthermore, to study the influence of the CPTu penetration rate on the inversion of the friction angle, according to the discriminant method and the characteristics of soil layer data, the stable values of tip resistance under different penetration rates in HRD silts were selected for parameter inversion in this experiment. The results are shown in Table. 4.

Table 4. Friction angle (φ') derived from cone penetration test

Penetration rate	20 mm/s	10 mm/s	1 mm/s	0.2 mm/s
φ' (Mayne)	34.34	32.43	28.41	27.65
φ' (Kulhawy)	31.69	30.297 9	27.54	27.05

Table 5. Fiction angle corresponding to surface sediment types in the Huanghe River Delta

Soil types	φ'/(°)	Data source
Normally consolidated silty soil	26.5–38.3	Meng et al., 2008; Liu, 2014; Lu and Li, 2003; Liu et al., 2006; Chang, 2009; Cheng, 2007; Liu et al., 2009; Wang et al., (2014
Sandy silt	32.5–38.3	Chang, 2009; Jia et al., 2011
Silty sand	38.0–42.6	

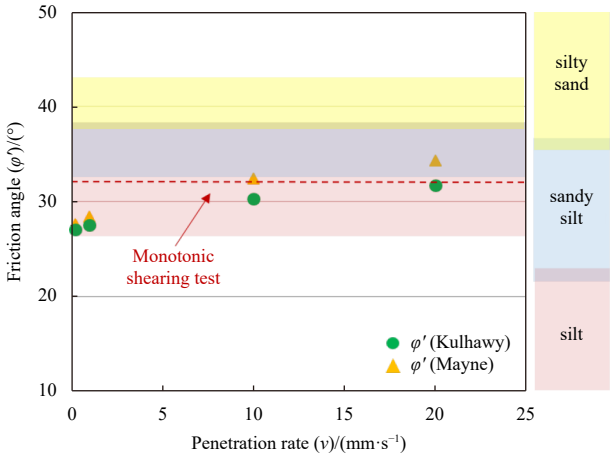

Fig. 11. Influence of CPTu penetration rate on friction angle.

Table 5 shows the friction angle of 10 m sediment in the HRD according to previous research.

Figure 11 shows the effect of the CPTu penetration rate on the friction angle obtained by data inversion.

The results show that the friction angle obtained by inversion at different rates approximately matches the range of reference values obtained by investigation. If the standard penetration rate is used for the penetration test, the value is overestimated compared with the low rate CPTu test. In this experiment, the inversion formula provided by Mayne (2006) appears to overestimate the friction angle of soil. Under the standard penetration rate, the friction angle inversion formula proposed by Kulhawy and Mayne (1990) is closer to the value obtained by the monotonic simple shear test. To some extent, the inversion results of friction angle depend on the CPTu penetration rate. It can be seen from Fig. 11 that the peak internal friction angle obtained by inversion increases with the increase of penetration rate, which is because different penetration rates lead to different drainage conditions. In this kind of HRD silts, the tip resistance increases as the penetration rate increases from 0.02 mm/s to 20 mm/s. Yang et al. (2022) conducted the CPT penetration tests in the HRD at a penetration rate of 20 mm/s to study the inversion of friction angle of HRD silts. To overcome the uncertainty involved in selecting design strength values for engineering designs with higher requirements, it is strongly recommended to conduct at least one fast and slow CPTu test to evaluate drainage conditions and adjust design values accordingly.

4.2 *Clay content effect*

To simulate silt with different clay contents near and far from the coast of the HRD, the CPTu penetration test data of different clays are designed and carried out. The results of q_t vs. h , Δu vs. h are shown in Fig. 12. The CPTu penetration test of the remolded soil samples showed that as the penetration rate increased from 0.2 mm/s to 20 mm/s, the tip resistance q_t gradually increased, and the pore pressure Δu gradually decreased. The measured values were similar when the penetration rates were 1 mm/s and 0.2 mm/s. In particular, when the penetration rate was 20 mm/s, the soil accumulates higher negative pore pressure; Fig. 12b shows the penetration test results of the silt samples containing 20% clay. In this case, as the penetration rate increases from 1 mm/s to 20 mm/s, the q_t increases with the increase of v. The tip resistance is the largest at the slowest penetration rate of 0.2 mm/s. This is because the silt sample contains 20% clay, and the rate effect is not obvious. The soil sample is partially drained at a low penetration rate. With the increase of the tip resistance, the penetration resistance q_t decreases gradually. The penetration resistance q_t measured at v = 10 mm/s and v = 1 mm/s are similar, which indicates that the soil is close to being completely undrained, and the tip resistance q_t is not affected by the penetration rate v. With the increase of penetration rate, when $v \geqslant 10$ mm/s, the soil is close to being completely drained, and the positive and negative pore pressure dissipates to zero, presenting the original water pressure. The silt samples containing 30% clay particles show complete drainage at the penetration rates of 20 mm/s, 10 mm/s and 1 mm/s, and the tip resistance q_t is almost equal. The pore pressure of the soil does not dissipate to 0 due to the influence of dilatancy.

The tip resistance is below 10 MPa because of the higher water pressure generated by the cone tip during the undrained process. The sleeve friction resistance is mostly below 100 kPa, because the HRD region has sensitive fine soils such as silty clay (Librić et al., 2017).

The tip resistance value and pore pressure value obtained in the stable section are normalized. The normalized cone tip resistance is shown in Eq. (8), and the normalized pore pressure is calculated in Eq. (2).

$$Q_t = \frac{q_t - \sigma_{v0}}{\sigma'_{v0}}, \tag{8}$$

where σ_{v0} and σ'_{v0} is the total overburden pressure and effective overburden pressure, respectively.

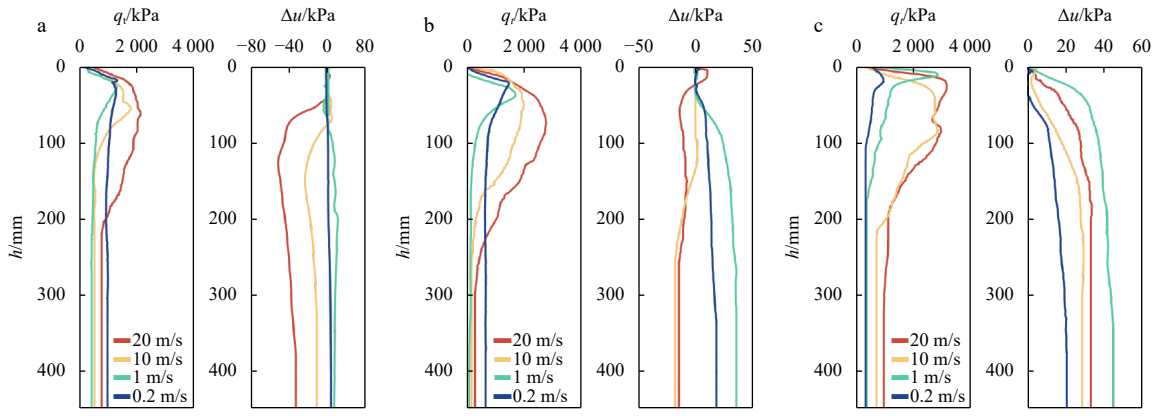

Fig. 12. Test results under different penetration rates in Huanghe River Delta (HRD) silts with different clay content: remolded HRD silts (a); 20% C (clay) mixture (b); 30% C (clay) mixture (c).

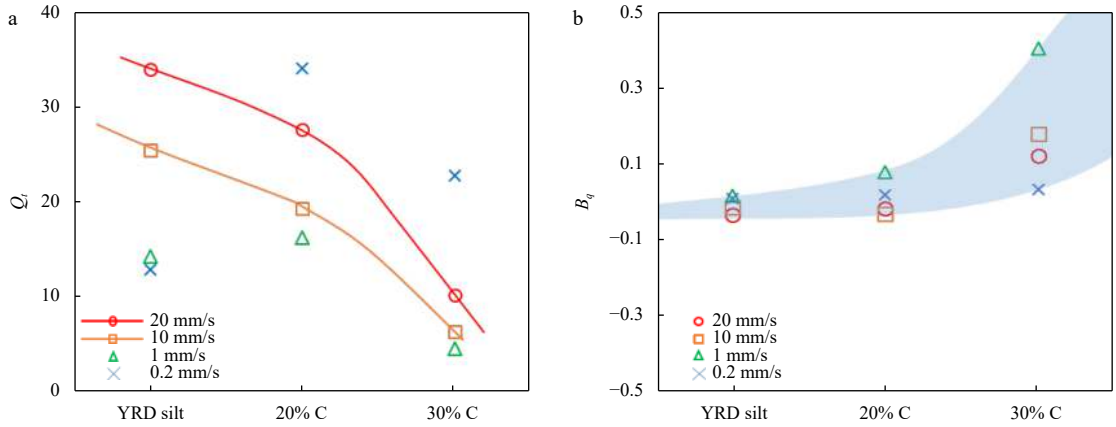

Fig. 13. Clay contents effect curves of silt and clay mixtures with different penetration rate: Q_t vs. clay content (a); B_q vs. clay content (b).

Figure 13 shows that, under different CPTu penetration rates, the tip resistance Q_t is strongly dependent on the clay content of the silt and varies with the penetration rate. The penetration rate effect in the penetration process is obvious. This study suggests that the standard penetration rate of 20 mm/s should be used when the CPTu is used to detect the clay content of silt in the HRD. The B_q value of the HRD silts is small, indicating that partial drainage has little effect on the test results. The influence of clay content on the pore pressure of silt in the HRD is mainly reflected in that as the clay content of the silt in the HRD increases, the distribution range of B_q widens, that is, the influence of the penetration rate on the test results increases with the increase of clay content. Moreover, when the penetration rate is slow, B_q converges to 0, corresponding to the complete drainage response in which all the excess pore pressure dissipates.

4.3 *CPT-based soil behaviour type classification*

The application of the piezocone penetration test in soil behaviour type classification is generally based on the analysis of the data obtained from the CPTu penetration experiment. As mentioned above, the researchable stable section data in this experiment is in the range of 200–450 mm penetration depth. Therefore, this paper selects the data of the stable section for analysis. Since most of the soil behaviour type classification methods proposed by predecessors and the field CPTu penetration experiment were carried out at the standard penetration rate of 20 mm/s, therefore, the experimental data of the standard penetration rate of 20 mm/s in pressure chamber tests were analyzed first to find a soil behaviour type classification method suitable for silt with different clay contents near and far away from the HRD. Meanwhile, the applicability of other penetration rates was tested to find the recommended penetration rate for the soil behaviour type classification of silt in the HRD.

According to the normal parameters of the commonly used analysis diagram, curves of cone-tip resistance q_t, and penetration depth, side friction resistance f_s and penetration depth of silt with different clay content under the standard penetration rate are shown in Fig. 14. According to the CPTu results, there is a certain regularity in homogeneous soil. It can be seen that the friction resistance of the sleeve changes within a certain depth range, mostly below 100 kPa.

Before analysing the soil behavior type classification, as shown in Fig. 15, the relationship between the penetration depth and the CPTu parameters were established to show the characteristics of the soil and find the soil behaviour types that usually have the characteristics. In this test data, the friction ratio ranges

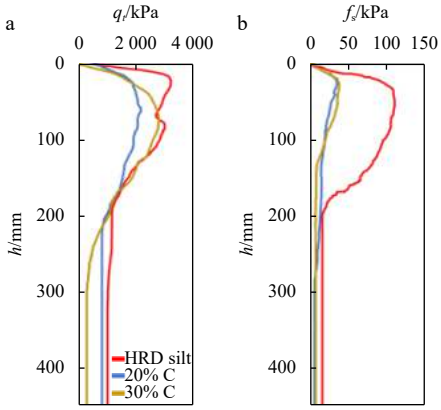

Fig. 14. Test results for Huanghe River Delta (HRD) silts with different clay contents: q_t vs. h (a); f_s vs. h (b).

from 1% to 3.3%, with an average of 2%, indicating that the soil behaviour type is mainly silty clay and silty soil. The value of normalized pore pressure B_q can be used to distinguish soil behaviour types. B_q value is close to 0 in the HRD silts (Zhang et al., 2022b).

The methods to calculate friction ratio R_f is as follows:

$$R_f = \frac{f_s}{q_c} \times 100\% . \tag{9}$$

4.3.1 *Robertson 1986 soil behaviour type classification chart*

The Robertson 1986 soil behaviour type classification method includes two charts q_t vs. R_f and q_t vs. B_q. The two charts can be used separately, and the q_t vs. R_f diagram is generally used. The soil was divided into 12 categories using the Robertson 1986 soil behaviour type classification method, as shown in Table 6.

Figure 16 shows the result of soil behaviour type classification using the Robertson 1986 soil behaviour type classification chart. At the standard penetration rate, the data points of the HRD soil and 20% C (the remolded HRD soil containing 20% clay content) are concentrated in Region 5 (clayey silt-silty clay). The data points of 30% C (the remolded HRD soil containing 30% clay content) are concentrated in Region 3 (clay), Region 4 (silty clay–clay). It can be seen that the soil behaviour type classification chart is suitable for the silt in the HRD and can identify the change of soil viscosity well.

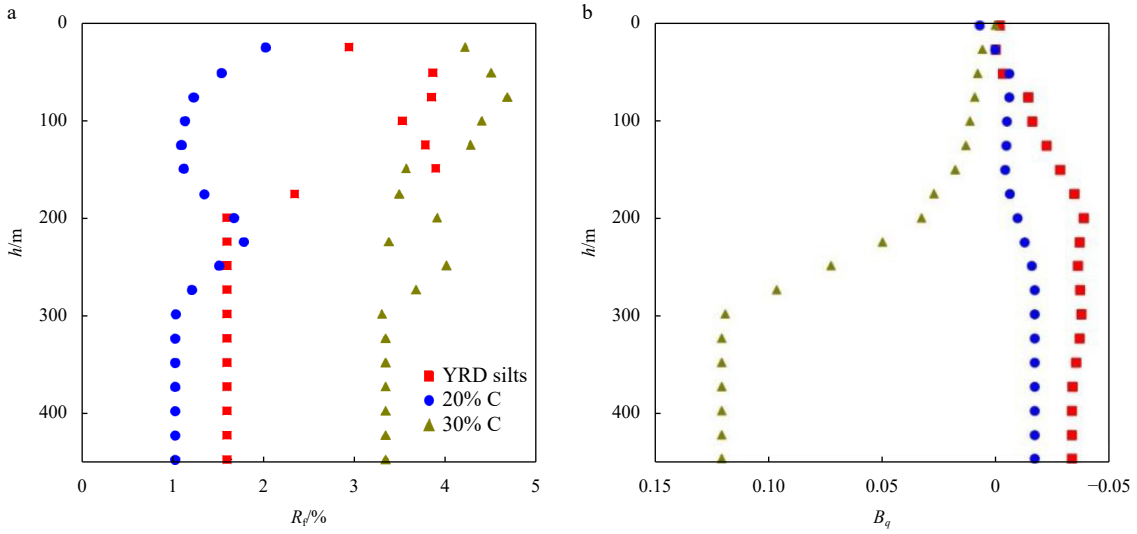

Fig. 15. Results of penetration experiment: depth distribution of friction ratio (a) ; depth distribution of B_q (b).

Table 6. Soil behaviour type classification

Region	Soil type	Region	Soil type
1	sensitive fine-grained soil	7	silty sand-sandy silt
2	organic soil	8	sand-silty sand
3	clay	9	sand
4	silty clay-clay	10	gravel sand-sand
5	clayey silt-silty clay	11	very stiff fine-grained soil*
6	sandy silt-clayey silt	12	sand-clayey sand*

Note: * refers to overconsolidated soil or cemented soil.

4.3.2 *Robertson 1990 chart and Robertson 2010 chart*

Figure 17 shows the results of soil behaviour type classification presented by Robertson 1990 and Robertson 2010, respectively. Table 7 shows the soil behaviour types corresponding to different areas of the chart.

The formula for calculating the normalized friction ratio is as follows:

$$F_r = \frac{f_s}{q_t - \sigma'_{v0}} \times 100\%. \tag{10}$$

According to the Robertson 1990 soil behaviour type classification chart, the data points of the HRD soil and 20% C are mainly concentrated in Region 5 (silty sand–sandy silt), 30% C is mainly concentrated in Region 3 (clay-silty clay) at the standard penetration rate. According to the Robertson 2010 soil behaviour type classification chart, the data points of the HRD soil and 20% C are mainly concentrated in Region 4 (clayey silt–silty clay). The data points of 30% C are divided into Region 3 (clay-silty clay) at the standard penetration rate. It can be seen that the accuracy of the Robertson 2010 soil behaviour type classification chart for silt is higher than that of the Robertson 1990 soil behaviour type classification chart. These two soil classification methods can identify the condition with relatively high clay content.

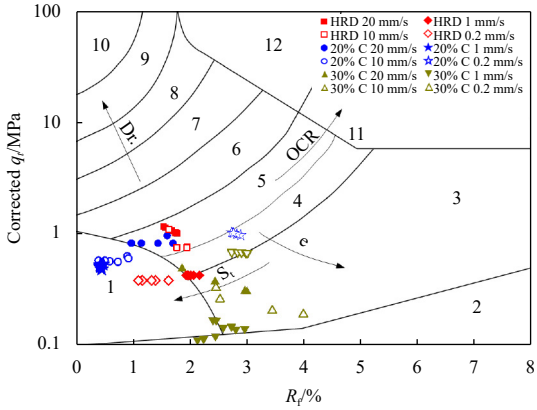

Fig. 16. Result of soil behaviour type classification using the Robertson 1986 chart.

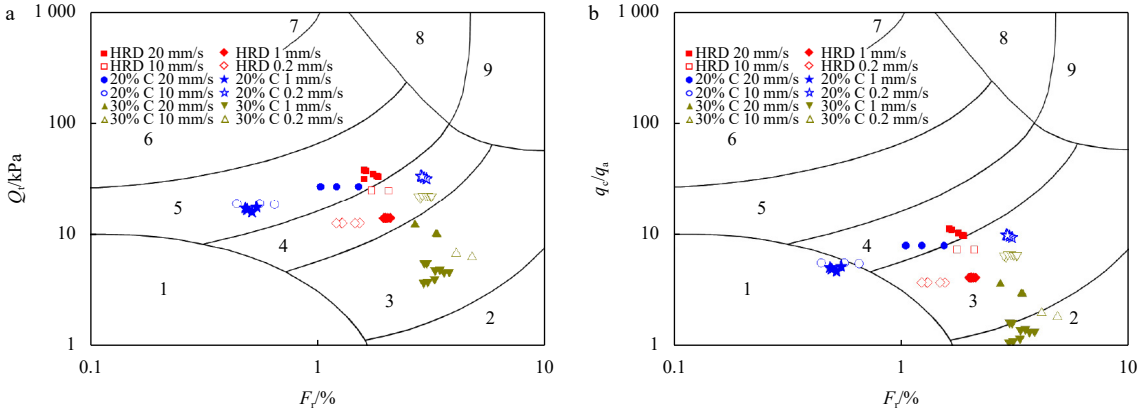

Fig. 17. Result of soil behaviour type classification using: the Robertson 1990 chart (a) and the Robertson 2010 chart (b).

Table 7. Soil behaviour type classification

Region	Soil type	Region	Soil type
1	sensitive fine-grained soil	6	sand-silty san
2	organic soil, peats	7	gravelly sand-sand
3	clay-silty clay	8	very stiff sand-clayey sand*
4	clayey silt-silty clay	9	very stiff, fine grained*
5	silty sand-sandy silt		

Note: * refers to overconsolidated soil or cemented soil.

Jefferies and Davies (1991) integrated Robertson's Q_t–F_r and Q_t–B_q soil type classification chart into a modified soil behaviour type classification chart represented by $Q_t(1–B_q)$–F_r. Subsequently, Jefferies and Davies (1993) proposed that the curve cluster of the soil behaviour type classification chart proposed after considering Q_t, B_q and F_r can be approximately estimated by concentric circles, and the radius of the circles is defined as the soil behaviour type index I_c, denoted as $I_{c(JD)}$. The expression is shown in Eq. (11),

$$I_{c(JD)} = \sqrt{((3 - \lg(Q_t(1 - B_q))^2 + (1.5 + 1.3\lg F_r)^2)}. \quad (11)$$

The soil behaviour type index I_c was calculated based on the experimental data in this study. The range of the soil behaviour type index is determined from the data of the stable section after the penetration depth of 200–450 mm. As shown in Fig. 18, the soil behaviour type index is not applicable to the HRD soil regardless of the penetration rate, at the same time, when the clay content is higher in soil, the value of Δu is relatively high while the measured tip resistance is relatively low, so it's possible that the value of $(1–B_q)$ is less than 0, that is, the soil behaviour type index of soil cannot be calculated. In this case, the above formula is unsuitable.

Robertson and Wride (1998) focused on the normalization of the tip resistance and proposed a new soil behaviour type index $I_{c(RW)}$ based on the Robertson 1990 soil behaviour type classification chart, which is defined as follows:

$$I_{c(RW)} = \sqrt{(3.47 - \lg Q_{tn})^2 + (1.22 + \lg F_r)^2}. \quad (12)$$

Robertson (2009) updated the normalized tip resistance Q_{tn} using a normalization with a variable stress exponent:

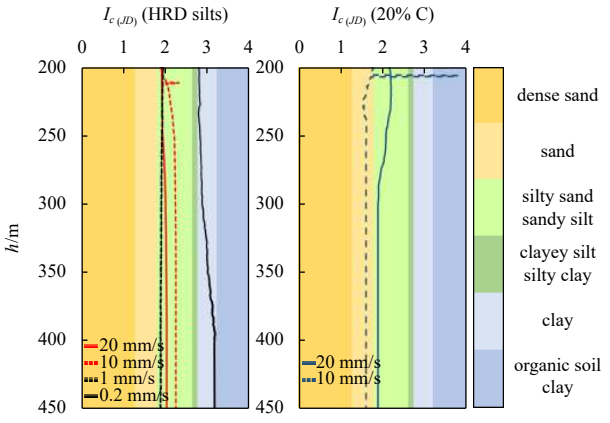

Fig. 18. Soil behaviour type classification for test points based on $I_{c(JD)}$.

$$Q_{tn} = \left(\frac{q_t - \sigma_{v0}}{p_a}\right) \times (p_a/\sigma'_{v0})^n. \quad (13)$$

In the Eq. (13), n is the stress exponent, and defined by

$$n = 0.381 I_{c(RW)} + 0.05(\sigma' v_0/p_a) - 0.15, \quad (14)$$

where $n \leqslant 1.0$.

Robertson (2010) proposed the I_{SBT} formula for rapid calculation of soil types based on the Robertson 2010 soil behaviour type classification chart. The formula is as follows:

$$I_{SBT} = \sqrt{\left(3.47 - \lg\left(\frac{q_c}{p_a}\right)\right)^2 + (1.22 + \lg F_r)^2}. \quad (15)$$

When the CPTu is used for testing, q_t can be used instead of q_c, to eliminate the influence of pore pressure at the permeable stone on the probe, and q_c can be used directly as it has little effect on the results.

Robertson proposed two parameters, $I_{c(RW)}$ and I_{SBT}, to identify soil behaviour type based on soil behavior type index. The method calculated $I_{c(RW)}$ uses the iterative calculation of normalized tip resistance Q_{tn} that considering the difference between cohesive soil and non-cohesive soil and is more reasonable than Q_t. This difference is more obvious in the non-cohesive soil area.

In this study, two soil behavior type indexes $I_{c(RW)}$ and I_{SBT} of the experimental soil are calculated. To facilitate visual judgement, a soil behavior type index chart was established that uses colour to distinguish different region. The results are shown in Figs 19 and 20. The range of the soil behavior type index is determined from the data of the stable section after the penetration depth of 200–450 mm. According to the $I_{c(RW)}$, the HRD soil and 20% C are in the region of silty sand-sandy silty, 30% C is in the region of clay at the standard penetration rate. According to the I_{SBT}, the HRD soil and 20% C are in the region of silty soil–clayey silt, 30% C is in the region of clay region at the standard penetration rate.

For HRD soil, the accuracy of soil behavior type classification using the I_{SBT} is higher than that of the $I_{c(RW)}$. This is because the large dilatancy of shallow HRD silts has an impact on the acquisition of the penetration resistance value. However, for the soil behavior type index $I_{c(RW)}$, the dilatancy influence is not taken into account in the calculation, and so the $I_{c(RW)}$ calculated under the condition of large q_t is smaller than the actual situation. Although the soil behavior type index I_{SBT} is more suitable for silt in the HRD, there are some errors and uncertainties. At the same time, when the clay content of the HRD soil is relatively low, the effect of penetration rate on the calculation of the behavior type indexes is not great. But for $I_{c(RW)}$, it just corresponds to two different soil types.

4.3.3 *Eslami classification chart*

The CPTu data of this study were projected onto the Eslami soil behaviour type classification chart and the obtained results are shown in Fig. 21. Most of the data points entered Region 2 (soft clay-soft silt), when the penetration rate is slow, some data points fall into Region 1 (collapsible soil-sensitive soil). The Eslami soil behaviour type classification chart can roughly identify the general types of soil, but cannot distinguish the clay content.

4.3.4 *Brouwer classification chart*

The CPTu data of this study were projected onto the Brouwer

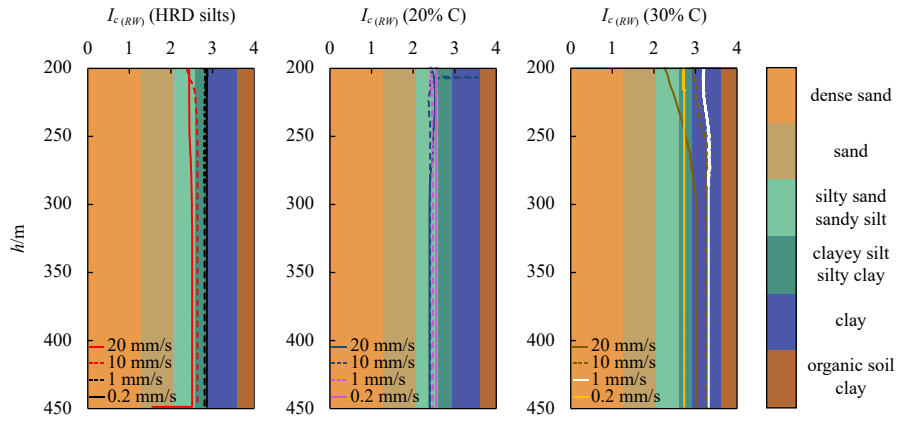

Fig. 19. Soil behaviour type classification for test points based on $I_{c(RW)}$.

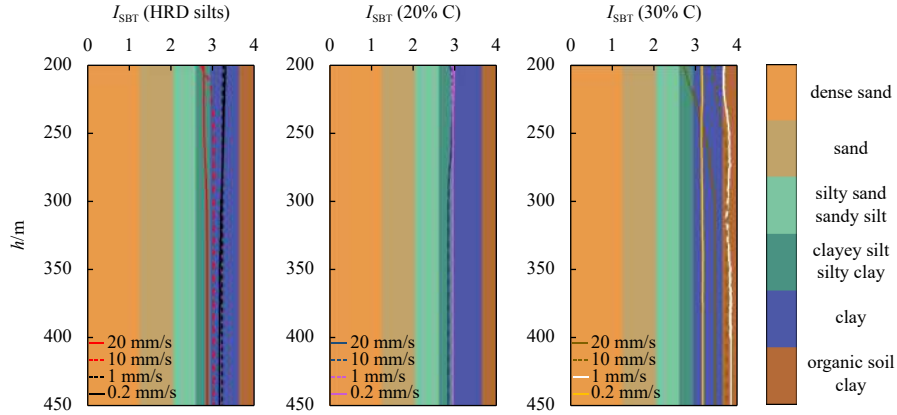

Fig. 20. Soil behaviour type classification for test points based on I_{SBT}.

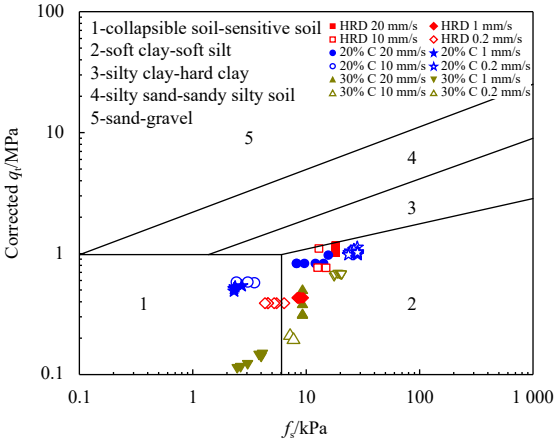

Fig. 21. Result of soil behaviour type classification using the Eslami classification chart.

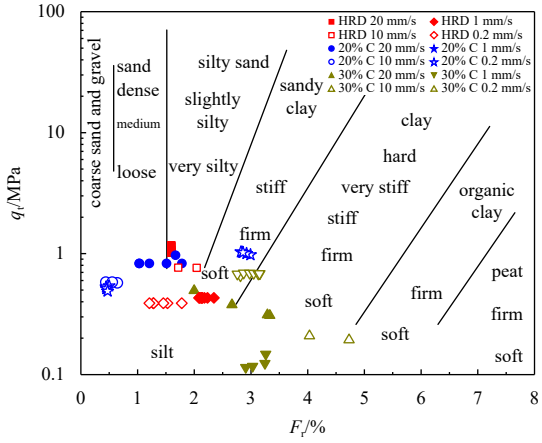

Fig. 22. Result of soil behaviour type classification using the Brouwer classification chart.

soil behaviour type classification diagram (Fig. 22). Some data points are in the silty soil region, and a small number of data points are in the silty sand regions. Similarly, penetration rate does not affect the results too much in this chart. The accuracy of the Brouwer soil behaviour type classification chart is lower than that of the others.

5 Conclusions

This study explored the characteristics of silt in the shoal area of the HRD through the laboratory monotonic shearing test and the CPTu variable rate penetration test. The friction angle was calculated through the monotonic simple shear test and was compared with the inversion results of the CPTu penetration test. The influence of penetration rate on the friction angle inversion is obtained, and some engineering suggestions were given. The effects of clay content on tip resistance and the pore pressure of silt under different penetration rates were summarized. The recommended penetration rate of CPTu for determination of clay content of the HRD silt is suggested. And the study analysed the applicability of five CPT-based soil behaviour type classification

charts and three soil behaviour type indexes to the soil with different clay contents of the HRD. The results provide a reference for strength parameter inversion of silty soil in the HRD and *in-situ* soil behaviour type classification. The specific conclusions are as follows:

(1) The penetration rate of the CPTu has a significant influence on the inversion of friction angle. In the standard rate penetration test, the friction angle calculated by the inversion formula proposed by Kulhawy and Mayne (1990) will be closer to the value obtained by the laboratory monotonic simple shear test for the silty soil with constant consolidation in the HRD. The peak internal friction angle obtained by inversion increases with the increase of penetration rate.

(2) The penetration rate effect in the penetration process is obvious. The tip resistance is strongly dependent on the clay content of the silt. It is suggested that the standard penetration rate of 20 mm/s should be used when CPTu is used to detect the clay content of silt in the HRD. The results show that the B_q value of HRD silts tends to 0 and is not significantly affected by the change of the CPTu penetration rate.

(3) The results show that a CPT-based soil behaviour type classification method can be used to analyse soil behaviour types, but the accuracy and applicability of specific methods need to be tested. In this study, the soil behaviour type classification methods based on the soil behaviour type index I_{SBT}, the Robertson 2010 were found to be more suitable for the silty soil in HRD. It is recommended to use the standard penetration rate when using CPTu for the soil behaviour type classification in the HRD.

References

Albatal A, Stark N, Castellanos B. 2020. Estimating *in situ* relative density and friction angle of nearshore sand from portable free-fall penetrometer tests. Canadian Geotechnical Journal, 57(1): 17–31, doi: 10.1139/cgj-2018-0267

Begemann H K S. 1965. The friction jacket cone as an aid in determining the soil profile. In: Proceedings of the 6th International Conference on Soil Mechanics and Foundation Engineering. Montreal: Springer, 17–20

Brandon T L, Rose A T, Duncan J M. 2006. Drained and undrained strength interpretation for low-plasticity silts. Journal of Geotechnical & Geoenvironmental Engineering, 132(2): 250–257

Brouwer H. 2007. *In Situ* Soil Testing. East Sussex: Lankelma, 144

Cai Guojun, Liu Songyu, Puppala A J. 2011. Comparison of CPT charts for soil classification using PCPT data: example from clay deposits in Jiangsu Province, China. Engineering Geology, 121(1–2): 89–96, doi: 10.1016/j.enggeo.2011.04.016

Chang Fangqiang. 2009. Study on mechanism of wave-induced submarine landslide at the Yellow River Estuary, China (in Chinese)[dissertation]. Qingdao: Ocean University of China

Cheng Chao. 2007. Research on liquefaction evaluation criteria for silty soil in Yellow River Delta (in Chinese)[dissertation]. Qingdao: Ocean University of China

Cheng Guodong, Xue Chunting. 1997. Sedimentary Geology of the Yellow River Delta (in Chinese). Beijing: Geological Publishing House

Douglas B J, Olsen R S. 1981. Soil classification using electric cone penetrometer. In: Proceedings of Conference on Cone Penetration Testing and Experience. St. Louis: ASCE, 209–227

Eslami A, Fellenius B H. 1997. Pile capacity by direct CPT and CPTu methods applied to 102 case histories. Canadian Geotechnical Journal, 34(6): 886–904, doi: 10.1139/t97-056

Feng Xiuli, Ye Yincan, Ma Yanxia, et al. 2002. Silt pore pressure response and dynamic strength under dynamic loading. Journal of Ocean University of Qingdao (in Chinese), 32(3): 429–433

Finke K A, Mayne P W, Klopp R A. 2001. Piezocone penetration testing in Atlantic Piedmont residuum. Journal of Geotechnical and Geoenvironmental Engineering, 127(1): 48–54, doi: 10.1061/(ASCE)1090-0241(2001)127:1(48)

Geiser F, Laloui L, Vulliet L. 2006. Elasto-plasticity of unsaturated soils: laboratory test results on a remoulded silt. Soils and Foundations, 46(5): 545–556, doi: 10.3208/sandf.46.545

Holmsgaard R, Ibsen L B, Nielsen B N. 2016. Interpretation of seismic cone penetration testing in silty soil. Electronic Journal of Geotechnical Engineering, 21(15): 4759–4779

Jefferies M G, Davies M P. 1991. Soil classification by the cone penetration test: Discussion. Canadian Geotechnical Journal, 28(1): 173–176, doi: 10.1139/t91-023

Jefferies M G, Davies M P. 1993. Use of CPTU to estimate equivalent SPT N60. Geotechnical Testing Journal, 16(4): 458–468, doi: 10.1520/GTJ10286J

Jia Yonggang, Shan Hongxian, Yang Xiujuan, et al. 2011. Sediment Dynamics and Geologic Hazards in the Estuary of Yellow River, China (in Chinese). Beijing: Science Press

Jones G A, Rust E. 1982. Piezometer penetration testing CUPT. In: 2nd European Symposium on Penetration Testing. Amsterdam: CRC Press, 607–613

Kulhawy F H, Mayne P W. 1990. Manual on estimating soil properties for foundation design. Palo Alto, CA: Electric Power Research Institute

Librić L, Jurić-Kaćunić D, Kovačević M S. 2017. Application of Cone Penetration Test (Cpt) Results for Soil Classification. Građevinar, 69(1): 11–20

Liu Jie. 2014. Analysis of consolidation settlement and its contribution to topographical change in the Modern Yellow River subaqueous delta (in Chinese)[dissertation]. Qingdao: Ocean University of China

Liu Xiaoyu, Liu Huixin, Sun Yongfu, et al. 2012. Experimental study of pore water pressure development mode of silt with different clay content under dynamic load. Coastal Engineering (in Chinese), 31(1): 1–7

Liu Hongjun, Lü Wenfang, Yang Junjie, et al. 2009. Influence of initial dry density and clay content on steady state strength of silty soil in Yellow River Delta. Chinese Journal of Geotechnical Engineering (in Chinese), 31(8): 1287–1291

Liu Shengfa, Zhuang Zhenye, Lü Haiqing, et al. 2006. The strata and environmental evolution in the late quaternary in the Chengdao area and modern Yellow River Delt Coast. Transactions of Oceanology and Limnology (in Chinese), 2006(4): 32–37

Long M. 2008. Design parameters from *in situ* tests in soft ground—recent developments. In: Geotechnical and Geophysical Site Characterization. London: CRC Press, 89–116

Lu Hongyou, Li Guangxue. 2003. The features of scouring and silting and the prediction of water depth in the Chengdao area of the Yellow River Delta in recent years. Journal of Chang'an University: Earth Science Edition (in Chinese), 25(1): 57–61

Lunne T, Christoffersen H P. 1983. Interpretation of cone penetrometer data for offshore sands. In: Proceedings of the Annual Offshore Technology Conference. Richardson, Texas: 181–192

Mayne P W. 2006. The Second James K. Mitchell Lecture Undisturbed sand strength from seismic cone tests. Geomechanics and Geoengineering, 1(4): 239–257, doi: 10.1080/17486020601035657

Meng Xiangmei, Jia Yonggang, Liu Xiaoli. 2008. Study on zoning and liquefaction induced by wave of Chengdao in Yellow River Delta. Journal of Engineering Geology (in Chinese), 16(S1): 44–53

Mitchell J K, Lunne T A. 1978. Cone resistance as measure of sand strength. Journal of the Geotechnical Engineering Division, 104(7): 995–1012, doi: 10.1061/AJGEB6.0000676

Qi Shanzhong, Liu Haili. 2017. Natural and anthropogenic hazards in the Yellow River Delta, China. Natural Hazards, 85(3): 1907–1911, doi: 10.1007/s11069-016-2638-9

Robertson P K. 1990. Soil classification using the cone penetration test. Canadian Geotechnical Journal, 27(1): 151–158, doi: 10.1139/t90-014

Robertson P K. 2009. Interpretation of cone penetration tests—a unified approach. Canadian Geotechnical Journal, 46(11): 1337–

1355, doi: 10.1139/T09-065

Robertson P K. 2010. Soil behaviour type from the CPT: an update. In: 2nd International Symposium on Cone Penetration Testing. Huntington Beach: Cone Penetration Testing Organizing Committee, 575–583

Robertson P K, Campanella R G. 1983. Interpretation of cone penetration tests. Part I: Sand. Canadian Geotechnical Journal, 20(4): 719–733

Robertson P K, Campanella R G, Gillespie D. 1986. Seismic CPT to measure *in situ* shear wave velocity. Journal of Geotechnical Engineering, 112(8): 791–803, doi: 10.1061/(ASCE)0733-9410(1986)112:8(791)

Robertson P K, Wride C E. 1998. Evaluating cyclic liquefaction potential using the cone penetration test. Canadian Geotechnical Journal, 35(3): 442–459, doi: 10.1139/t98-017

Senneset K, Janbu N. 1985. Shear strength parameters obtained from static cone penetration tests. In: Strength Testing of Marine sediments: Laboratory and *In-Situ* Measurement. West Conshohocken, PA: ASTM International, 41–54

Shahri A A, Malehmir A, Juhlin C. 2015. Soil classification analysis based on piezocone penetration test data—A case study from a quick-clay landslide site in southwestern Sweden. Engineering Geology, 189: 32–47, doi: 10.1016/j.enggeo.2015.01.022

Schneider J A, Randolph M F, Mayne P W, et al. 2008. Analysis of factors influencing soil classification using normalized piezocone tip resistance and pore pressure parameters. Journal of Geotechnical and Geoenvironmental Engineering, 134(11): 1569–1586, doi: 10.1061/(ASCE)1090-0241(2008)134:11(1569)

Song Binghui, Sun Yongfu, Song Yupeng, et al. 2020. Post-liquefaction re-compaction effect on the cyclic behavior of natural marine silty soil in the Yellow River Delta. Ocean Engineering, 195: 106753, doi: 10.1016/j.oceaneng.2019.106753

Suzuki Y. 2015. Investigation and interpretation of cone penetration rate effects [dissertation]. Crawley, WA, Australia: The University of Western Australia

Tonni L, Gottardi G. 2011. Analysis and interpretation of piezocone data on the silty soils of the Venetian lagoon (Treporti test site). Canadian Geotechnical Journal, 48(4): 616–633, doi: 10.1139/t10-085

Wang Hu, Liu Hongjun. 2016. Evaluation of storm wave-induced silty seabed instability and geo-hazards: A case study in the Yellow River Delta. Applied Ocean Research, 58: 135–145, doi: 10.1016/j.apor.2016.03.013

Wang Xiaohua, Liu Hongjun, Jia Yonggang. 2008. The research on the mineral characteristics of sediment and the responce to the hydrodynamic conditions of the tidal flat, at the northern Yellow River Delta. Marine Science (in Chinese), 32(2): 42–46

Wang Hu, Liu Hongjun, Zhang Minsheng, et al. 2014. Undrained shear strength behavior of ocean silt under low stress conditions and its application to analyzing submarine shallow landslides. Chinese Journal of Rock Mechanics and Engineering (in Chinese), 33(4): 849–856

Wen Mingzheng, Wang Zhenhao, Zhang Bowen, et al. 2018. Survey on the distribution of fluid mud and disturbed strata on subaqueous Yellow River Delta. Journal of Engineering Geology (in Chinese), 26(S1): 677–683

Yang Zhongnian, Liu Xuesen, Su Xiuting, et al. 2022. CPT-Based evaluation of sediment characteristics and effective internal friction angle in the Yellow River Estuary. Marine Georesources & Geotechnology, 40(9): 1108–1118

Yang Zhongnian, Zhu Yongmao, Liu Tao, et al. 2019. Pumping effect of wave-induced pore pressure on the development of fluid mud layer. Ocean Engineering, 189: 106391, doi: 10.1016/j.oceaneng.2019.106391

Zhang Yan, Feng Xiuli, Deng Shenggui, et al. 2022a. Pore pressure response and dissipation of piezocone test in shallow silty soil of Yellow River Delta. Journal of Marine Science and Engineering, 10(2): 225, doi: 10.3390/jmse10020225

Zhang Yan, Feng Xiuli, Ding Chenhao, et al. 2022b. Study of cone penetration rate effects in the Yellow River Delta silty soils with different clay contents and state parameters. Ocean Engineering, 250: 110982, doi: 10.1016/j.oceaneng.2022.110982

Zhang Jiarui, Meng Qingsheng, Zhang Yan, et al. 2022c. Effect of penetration rates on the piezocone penetration test in the Yellow River Delta silt. Journal of Ocean University of China, 21(2): 361–374, doi: 10.1007/s11802-022-4934-1